ACS APPLIED MATERIALS & INTERFACES

Research Article

www.acsami.org

Electrochemical Stability and Postmortem Studies of Pt/SiC Catalysts for Polymer Electrolyte Membrane Fuel Cells

Serban N. Stamatin,[†,§] Jozsef Speder,[‡] Rajnish Dhiman,*[,†] Matthias Arenz,[‡] and Eivind M. Skou[†]

[†]Department of Chemical Engineering, Biotechnology and Environmental Technology, University of Southern Denmark, Niels Bohrs Alle 1, DK-5230 Odense M, Denmark

[‡]Department of Chemistry and Nano Science Center, University of Copenhagen, Universitetsparken 5, DK-2100 Copenhagen, Denmark

Supporting Information

ABSTRACT: In the presented work, the electrochemical stability of platinized silicon carbide is studied. Postmortem transmission electron microscopy and X-ray photoelectron spectroscopy were used to document the change in the morphology and structure upon potential cycling of Pt/SiC catalysts. Two different potential cycle aging tests were used in order to accelerate the support corrosion, simulating start-up/shutdown and load cycling. On the basis of the results, we draw two main conclusions. First, platinized silicon carbide exhibits improved electrochemical stability over platinized active carbons. Second, silicon carbide undergoes at least mild oxidation if not even silicon leaching.

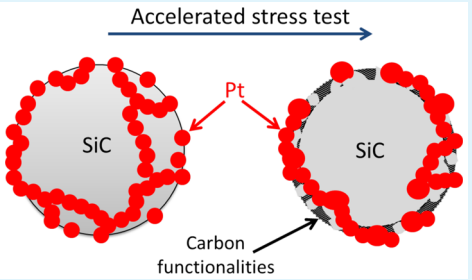

KEYWORDS: *electrochemical stability, electrochemical surface area, accelerated stress test, postmortem XPS, postmortem TEM, support corrosion*

1. INTRODUCTION

Electrochemical energy conversion and storage are of the utmost importance in future energy systems. The performance of such devices is governed by the electrochemical reactions taking place at the electrodes. Therefore, the activity and stability of the electrodes have a direct effect on the overall power output. Fuel cells are electrochemical energy devices that convert the energy of a fuel into useful energy. The reactions in polymer electrolyte membrane fuel cells (PEMFCs) take place at the surface of the catalyst, i.e., usually platinum in the form of nanoparticles that are supported on active carbons. Unfortunately, a key fuel cell performance loss is carbon corrosion, which has been established as a primary degradation phenomenon of the catalyst.[1] Several alternative carbon nanomaterials as support have been proposed to replace the active carbons.[2−5] However, at the applied conditions, carbon is thermodynamically unstable, and it is further reported that carbon nanostructures are undergoing mild corrosion in the presence of platinum, which promotes their degradation.[6,7] In this respect, carbides,[8−10] oxides,[11−13] and nitrides[14,15] have recently attracted wide interest because of their chemical inertness and possible interaction with platinum.

In the quest for stable electrocatalyst supports for phosphoric acid fuel cells, Honji et al. tested silicon carbide (SiC) as early as 1988.[16] The reasoning behind this was the good chemical stability of SiC in hot phosphoric acid. However, even though the sample exhibited potential−current density values similar to platinum (Pt)/carbon (C), no electrochemical stability studies followed. This early study[16] led to the use of nano-SiC as an electrocatalyst support for PEMFCs.[17] Lv et al. showed using postmortem electron microscopy that Pt/SiC/C has an improved electrochemical stability over Pt/C at potentials up to 1.2 V_{RHE}.[18] Nevertheless, support-related performance loss occurs at potentials as high as 1.5 V_{RHE}, which are encountered during start-up/shutdown periods, fuel starvation, or the reverse current region. Recently, silicon carbide−carbon (SiC−C) composites were tested as electrocatalyst supports for methanol oxidation and the oxygen reduction reaction (ORR).[18−20] Electrochemical stability studies showed a reduced degradation trend for SiC−C after 800 cycles.[19,20] It is well-known that the thermodynamic stability limitation of carbon in acidic media is at 0.207 V_{RHE}, as seen in its Pourbaix diagram.[21] Because of sluggish electrode kinetics, no carbon dioxide is formed at these low potentials. Nonetheless, corrosion is enhanced significantly at higher potentials. A similar trend was observed recently for titanium-coated SiC.[22] However, the use of active carbon or titanium, materials that are not stable in PEMFC operating conditions, in corroboration with a presumable stable material, such as SiC, does not seem to be the most self-evident solution. In the case of ceramic materials, electrochemical stability studies should be accompanied by surface chemistry characterization in order to reveal any surface composition change. This has proven useful for other carbides, such as tungsten carbide (WC), where above 0.8 V_{RHE} the WC transforms into at least two WO_x species, leading to significant platinum detachment.[23]

Received: December 23, 2014
Accepted: February 26, 2015
Published: February 26, 2015

DOI: 10.1021/am508982d
ACS Appl. Mater. Interfaces 2015, 7, 6153−6161

In our previous work, we reported on a synthesis method of Pt/SiC, in which the addition of carbon is not necessary.[24] The electrochemical activity values for methanol oxidation and the ORR were similar to those obtained for Pt/C.[25] In spite of the several studies concerned with the use of SiC as an electrocatalyst support, so far there is no work concerning the surface chemistry of Pt/SiC after extended cycling periods in simulated start-up/shutdown conditions (where carbon is known to corrode). Herein, we report for the first time the electrochemical stability of Pt/SiC and its change in surface chemistry upon simulated PEMFC operating conditions.

2. EXPERIMENTAL SECTION

2.1. Materials and Synthesis. SiC was synthesized using a method reported elsewhere.[26] Briefly, wooden samples were dried at 353 K for 4 h and heated to 773 at 1 K min^{-1} heating rate, followed by another heat treatment at 1473 K for 6 h at a heating rate of 5 K min^{-1}. The synthesis took place in a horizontal alumina-tube-lined furnace (Lenton Thermal Designs Ltd.). Argon was purged at 300 mL min^{-1}. After cooling to room temperature, silicon and silicon dioxide (99.5%, Sigma-Aldrich) were mixed in a 1:1 molar mixture and placed in an alumina crucible next to the pyrolyzed wood. Then, this was heated to 1723 at 5 K min^{-1} and dwelled for 16 h under a 300 mL min^{-1} argon flow. The obtained material contained a C−SiC mixture. This was placed in a funnel containing a 1:1 mixture of chloroform (99.9%, CHROMASOLV Plus, Sigma-Aldrich) and toluene (99.9%, CHROMASOLV Plus, Sigma-Aldrich). A two-phase solution was obtained after mechanical stirring, which allowed the separation of SiC from unreacted carbon. This procedure was repeated 10 times, and the resulting material was dried at 353 K for 12 h and denoted as SiC.

Prior to platinization, SiC followed an acid treatment described elsewhere.[24] The deposition of platinum was performed using a modified polyol method.[27] A total of 150 mg of SiC was added to 20 mL of ethylene glycol (99%, VWR) and mixed with 20 mL of a 9.6 mM K_2PtCl_4 (46.75% Pt, Alfa-Aesar)/ethylene glycol solution. The mixture was stirred for 30 min at room temperature and then refluxed at 423 K for 3 h under constant argon purging. After cooling to room temperature, Pt/SiC was cleaned five times by a 10 min centrifugation at 4500 rcf (Eppendorf 5804). The solvent was removed by drying for 12 h at 363 K. This procedure of platinization with given amounts of reactants produced 37 mg of metallic platinum on SiC, which translates into 20 wt % platinum in Pt/SiC.

2.2. Physicochemical Characterization. X-ray diffraction (XRD) was performed by means of a Siemens D-5000 X-ray diffractometer equipped with Cu Kα (1.5418 Å) and measured in the 2θ = 20−85° range with a 0.02° s^{-1} step and a 10 s $step^{-1}$ dwelling time.

X-ray photoelectron spectroscopy (XPS) was carried out using a SPECS spectrometer and a Mg Kα source (1253.2 eV). The survey spectra were measured in 200−1260 eV kinetic energy and had a resolution of 2.5 eV. The high-resolution spectra were recorded at a resolution of 1.3 eV. *CasaXPS* was used to deconvolute the peaks to pure Gaussians using a "Shirley" background. Peak deconvolution was performed similarly to our previous studies on Pt/SiC.[24,25]

The pristine and electrochemically treated electrocatalyst samples were characterized by transmission electron microscopy (TEM) using a Tecnai T20 G2 microscope (Philips FEI, Hillsboro, OR) equipped with a thermionic electron gun operated at 200 kV.

2.3. Electrochemical Stability Studies. An all-glass two-compartment three-electrode cell setup was used throughout this work. A 0.12 cm^2 gold plate was used as the working electrode. Catalyst inks were prepared by dispersing the required amount of catalyst in 5 mL of ultrapure water, suspending it over the working electrode, and leaving it to dry under an IR lamp. The platinum electrode loading was maintained at 125 μg_{Pt} cm_{geo}^{-2}. The counter electrode consisted of a platinum wire with approximately 40 windings and encapsulated in a glass tube with a bottom ceramic frit. A dynamic hydrogen electrode (Hydroflex, Gaskatel) was used as the reference electrode. A Pine Instrument bipotentiostat (operated in potentiostat mode) was used throughout this work. The aged materials deposited on gold electrodes were used for the postmortem XPS studies. Gold electrodes were used only for postmortem XPS analysis because of the convenience of mounting them on the XPS sample holder and then transfering them inside the UHV chamber. For postmortem TEM studies, a home-built multielectrode setup with eight glassy carbon electrodes was used as the working electrode and placed in an all-Teflon three-compartment electrochemical cell without stirring. The reference electrode [Schott Ag/AgCl/KCl(sat.)] was separated by a Nafion membrane,[28] and a graphite rod was used as the counter electrode. The electrodes were controlled by a potentiostat (Princeton Applied Research 263A). All potentials are referred to the reversible hydrogen electrode (RHE). The experiments took place at room temperature in approximately 200 mL of freshly prepared argon-saturated 0.1 M $HClO_4$ (TraceSelect, Sigma-Aldrich).

Two individual aging tests were used in order to test the electrochemical stability of Pt/SiC. These are well-known degradation protocols, proposed by the Fuel Cell Commercialization Conference of Japan (FCCJ), that separate the electrocatalyst degradation from the support degradation when two types of experiments are performed.[29] In the first step, herein denoted FCCJ I, the working electrode is exposed to a square-wave potential with two steps, 0.6 and 1 V_{RHE}, and a 3 s $step^{-1}$ hold, hence 6 s $cycle^{-1}$. In this work, the sample was subjected to 10000 cycles (approximately 17 h) and the electrochemical surface area (ESA; determined from H_{upd}[30]) was measured every 1000 cycles. In the other step, herein denoted as FCCJ II, the electrode is subjected to a triangular wave potential between 1 and 1.5 V_{RHE} at 0.5 V s^{-1} for 30000 cycles (approximately 17 h). In this case, the ESA was measured every 2500 cycles.

3. RESULTS AND DISCUSSION

3.1. Physicochemical Characterization. The successful deposition of metallic platinum on the SiC support is confirmed by the X-ray diffractogram shown in Figure 1.

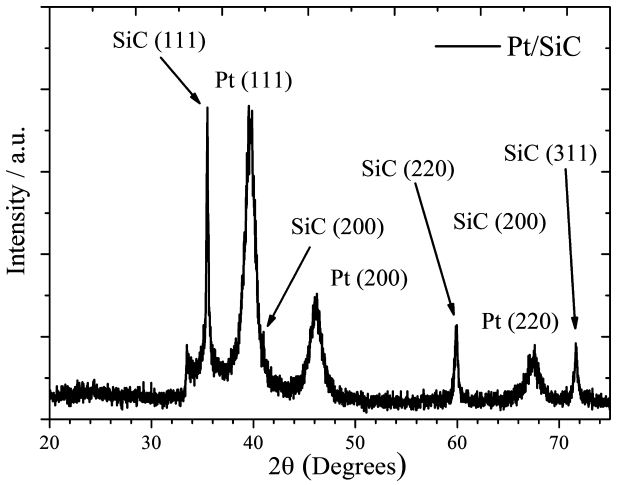

Figure 1. XRD pattern of the synthesized Pt/SiC catalysts. The individual diffraction peaks of the platinum and SiC support are assigned according to the International Centre for Diffraction Data PDF 00-029-1131 for platinum and 00-004-0802 for SiC.

Peaks corresponding to SiC(111), SiC(220), and SiC(311) are clearly observed at 2θ = 35.5°, 59.9°, and 71.7° (ICDD: 00-029-1131). Platinum characteristic peaks are observed at 2θ = 39.6°, 46.1°, and 67.4°, corresponding to the diffraction from Pt(111), Pt(200), and Pt(220). The platinum peaks are assigned according to the International Centre for Diffraction Data PDF 00-004-0802 and show a face-centered-cubic crystal structure for platinum. A double type of peak is observed for

DOI: 10.1021/am508982d
ACS Appl. Mater. Interfaces 2015, 7, 6153−6161

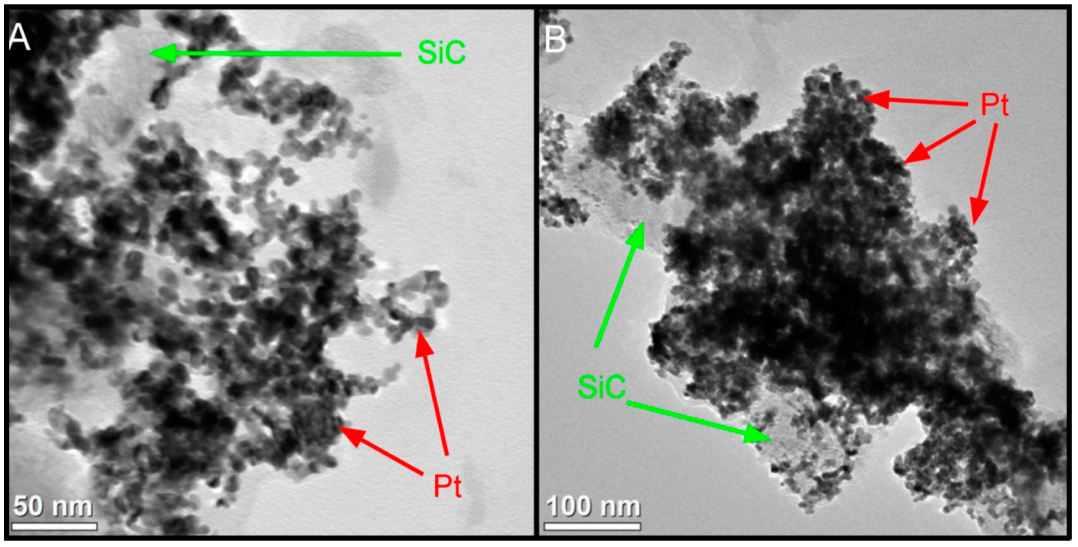

Figure 2. TEM micrographs of Pt/SiC at different magnifications, where platinum nanoparticles and SiC are marked by red and green arrows, respectively.

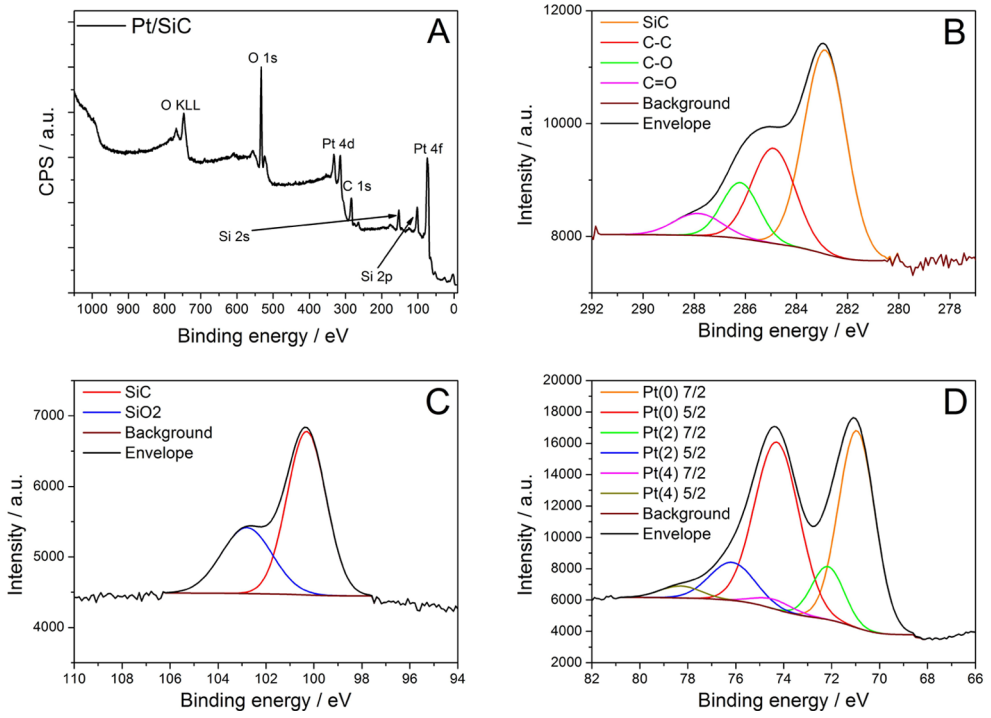

Figure 3. XPS survey spectrum of the prepared Pt/SiC catalyst ink (A) with high-resolution XPS of C 1s (B), Si 2p (C), and Pt 4f (D).

Pt(111), which is due to the SiC(200) situated at $2\theta = 41.2°$.[25] For this reason, the average platinum crystallite size was calculated from Pt(220) using the Scherrer formula, resulting in a size of approximately 5.7 nm.

TEM analysis was performed in order to observe the morphology of the obtained catalyst material. As seen, the SiC particle size is in the micrometer range, as was also reported in our previous studies.[24,25] Platinum nanoparticles are presented as dark particles supported on light-gray SiC, as seen in Figure 2. TEM indicated that the platinum nanoparticles appear as bunches on the SiC surface, forming an interconnected network. According to the platinum particle histogram obtained from TEM micrographs (Figure S1 in the Supporting Information, SI), the average particle size is approximately 5.8 ± 1.9 nm, which is in line with the crystallite size obtained from XRD.

The XPS survey of Pt/SiC (Figure 3A) reveals the presence of carbon, oxygen, silicon, and platinum. No other peaks are observed, indicating that no contaminants are present in the sample. The surface elemental composition as obtained from the XPS survey leads to a C/O/Si/Pt elemental composition of 29/28/33/10 (Table 1). That is the platinum content is only 10%, which is significantly lower than the expected 20% based on the ratio of used materials in the synthesis. This difference in composition could be due to the fact that XPS is a surface science technique that samples only the first few top nanometers of the sample. In addition, XPS indicates that the content of oxygen is rather high, which might suggest that SiC

DOI: 10.1021/am508982d
ACS Appl. Mater. Interfaces 2015, 7, 6153−6161

Table 1. Surface Elemental Composition (%) Obtained from XPS Analysis

	29% C 1s			28% O 1s		33% Si 2p		10% Pt 4f	
	SiC	C−C	OCG[a]	PtO_2	OCG[a]	SiC	SiO_2	Pt^0	Pt−O
Pt/SiC	54	26	20	14	86	66	34	77	23

[a]Oxygen-containing group.

is already oxidized. However, it should be taken into account that XPS was performed from a few drops of the catalyst ink, which contained Pt/SiC and water. The large fraction of oxygen might therefore come from surface-adsorbed water or organic impurities. In powder-based form, the XPS data are similar to those previously reported.[24,25]

The high-resolution XPS spectrum of the C 1s binding energy (Figure 3 B) reveals that the major component is SiC (Table 1), with a contribution of C−C. The large amount of C−C species might be due to some unreacted carbon left from the synthesis or from organic contaminants. Oxygen functional groups are present as well, and it is well-known that these are serving as nucleation sites for platinum.[31] Further, deconvolution of the O 1s peak indicates that some of the platinum surface (14%) is oxidized. Similar to the C 1s peak, the major component in the Si 2p peak comes from SiC. The ratio between SiC determined from C 1s and Si 2p peaks is approximately 1:1, which indicates a very pure SiC.[26] The Pt 4f high-resolution XPS spectrum confirms that most of the platinum is in metallic form, confirming that platinum reduction was successful.

3.2. Electrochemical Stability Studies. In the previous subsection, it was shown that platinum nanoparticles with an average size of 6 nm are evenly distributed on the surface of SiC. We have previously shown that Pt/SiC exhibits an electrochemical activity similar to commercially available Pt/C.[24,25] The purpose of this study is to investigate the electrochemical stability under simulated load cycles and start-up/shutdown conditions. In this respect, we have used a two-step degradation protocol as proposed by the FCCJ[29] and performed postmortem TEM and XPS studies in order to shed some light on the electrochemical stability of SiC.

Several differences are observed between the cyclic voltammetry (CV) at the beginning of test (BOT) and that at the end of test (EOT) in the case of Pt/SiC treated with the FCCJ protocol I (Figure 4A). The initial specific electrochemical surface area (ECSA) was 52.2 $m^2\ g_{Pt}^{-1}$ with a 2.3 standard error (SE), while the final ECSA was 41.7 $m^2\ g_{Pt}^{-1}$ with a 2.6 SE. The obtained ECSA is high in spite of the apparent agglomeration visible in Figure 2 and the relatively large platinum particle size. This translates into a loss in ESA of approximately 20% (Figure 4B). Furthermore, the platinum oxide region (blue circle in Figure 4A) exhibits a significant decrease as well. Consequently, the platinum oxide reduction region decreases in the cathodic sweep. At BOT, the peak current density in the cathodic sweep is situated at a potential of 0.75 V_{RHE}. At EOT, the peak potential is shifted toward larger values, indicating particle growth as a result of the degradation test. Such a behavior was previously also observed for carbon-based samples.[7,32,33] These differences in the CV at BOT and EOT were expected because of the fact that the FCCJ protocol I primarily degrades the active platinum nanoparticles, via a mixed degradation mechanism composed of platinum dissolution, agglomeration, growth, and Ostwald ripening. Therefore, changing the support should not result in increased stability of the catalyst, which is also consistent with previous

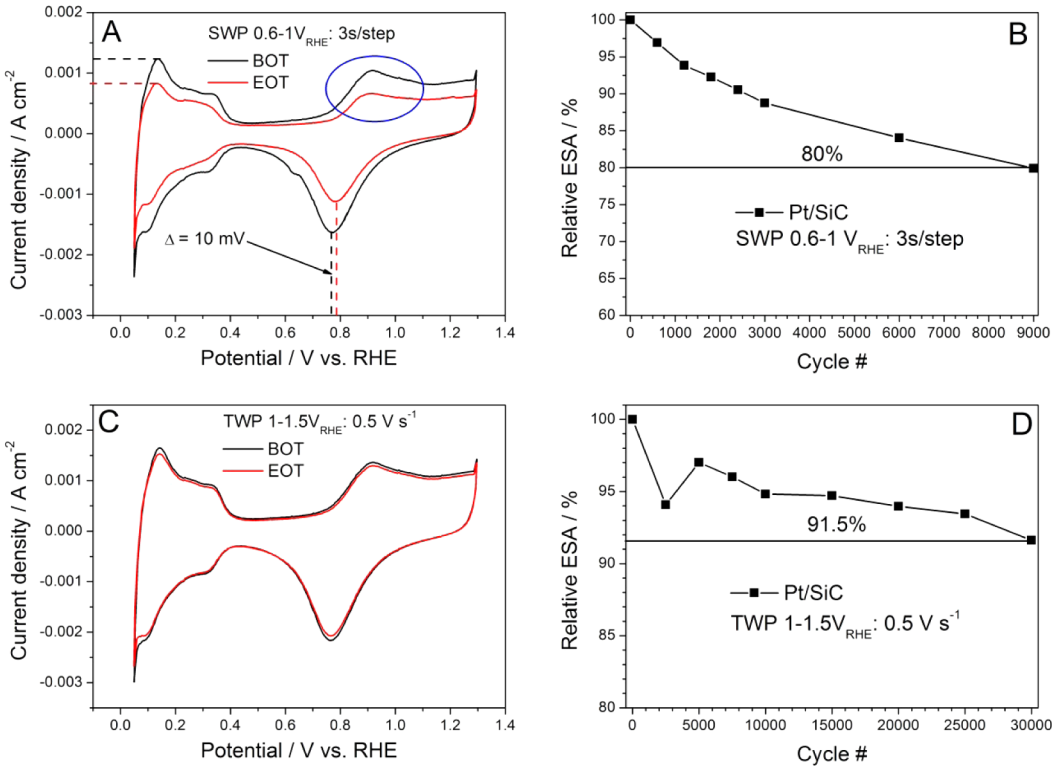

Figure 4. CVs at BOT (black line) and EOT (red line) of Pt/SiC treated with FCCJ I (A) and FCCJ II (C). Degradation profile of Pt/SiC during FCCJ I (B) and FCCJ II (D).

DOI: 10.1021/am508982d
ACS Appl. Mater. Interfaces 2015, 7, 6153−6161

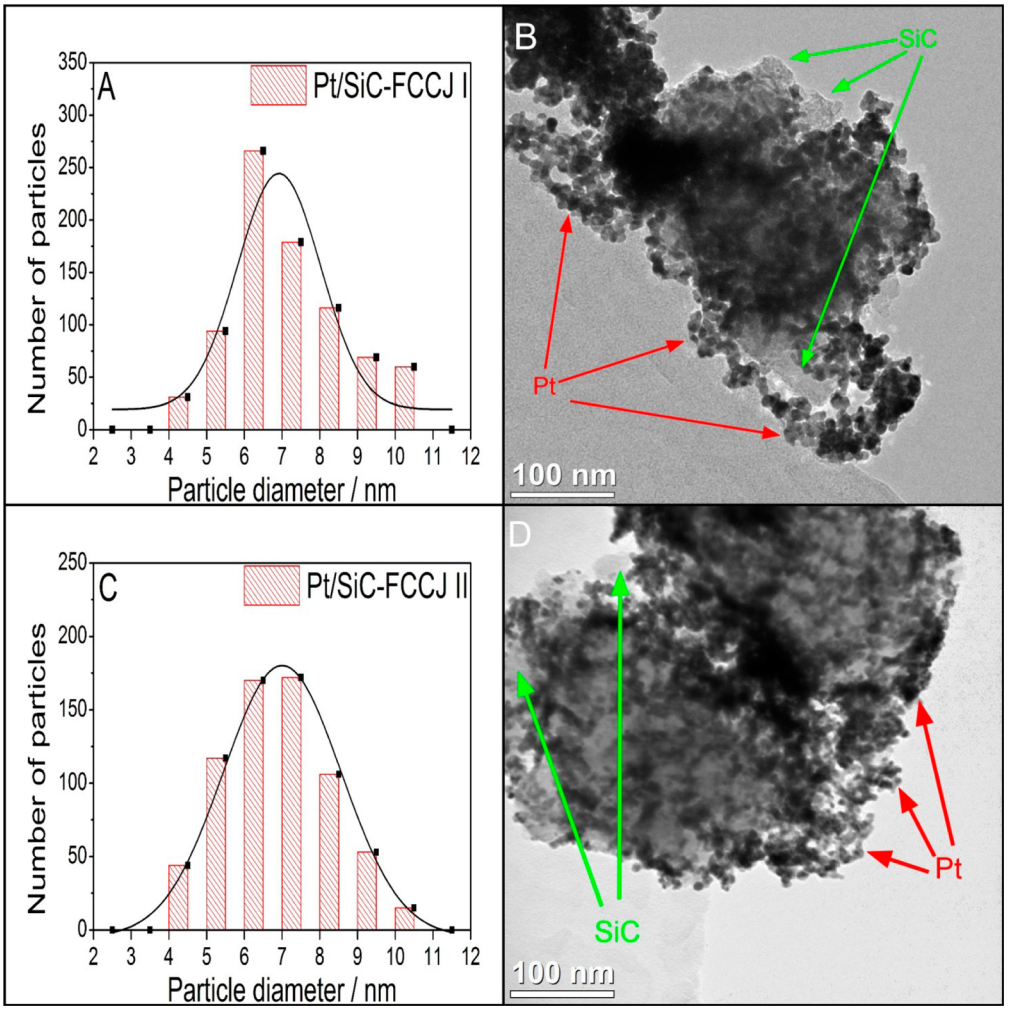

Figure 5. Particle histogram and postmortem TEM micrographs of Pt/SiC−SMS after 9000 cycles of FCCJ I (A and B) and 30000 cycles of FCCJ II (C and D). Particle histograms were created from measurement of more than 500 particles from several TEM locations. Green arrows indicate SiC, while red arrows indicate platinum nanoparticles. FCCJ I: square-wave potential with 3 s step^{-1} (6 s cycle^{-1}) at 0.6 and 1 V_{RHE} in argon-saturated 0.1 M $HClO_4$. FCCJ II: triangular-wave potential between 1 and 1.5 V_{RHE} at 0.5 V s^{-1} in argon-saturated 0.1 M $HClO_4$.

studies.[34] It is, however, interesting that an almost linear degradation behavior is observed, indicating that there is continuous loss in ESA and, hence, in the electrochemical performance. Furthermore, a larger loss in ESA (i.e., 40−50%) is observed for Pt/C degraded under similar conditions.[35,36] Even though one might ascribe the smaller ESA loss of Pt/SiC to a stabilizing effect of SiC, it should be taken into consideration that in the Pt/SiC catalyst the initial size of the platinum nanoparticles is larger than that in the Pt/C reference, and it is therefore expected that platinum is more stable.[37]

Upon application of the FCCJ protocol II, the Pt/SiC catalyst does not undergo severe electrochemical change (Figure 4C). The only difference observed in the CVs at BOT and EOT is a minor reduction in the current densities at EOT. While for Pt/C treated under similar conditions a large peak emerges between 0.5 and 0.7 V_{RHE}[36,38] that is associated with a quinone/hydroquinone couple, such behavior is not observed for Pt/SiC. Furthermore, no potential difference is observed in the platinum oxide reduction region as found for the sample treated with the FCCJ protocol I. Moreover, no additional peaks are observed in the CV that might suggest SiC oxidation. The initial ECSA was 53.9 m^2 g_{Pt}^{-1} with a 4.6 SE, while the final ECSA was 49.4 m^2 g_{Pt}^{-1} with a 3.8 SE. The degradation profile of Pt/SiC during FCCJ II (Figure 4D) shows that only 8.5% of the initial ESA is lost. This is remarkable considering that for amorphous carbon and multiwalled carbon nanotubes the ESA loss ranged between 10 and 20% under similar conditions.[7,33]

In order to determine the degradation mechanism, initially identical-location TEM was pursued. However, this was abandoned because of the very low SiC BET surface area (approximately 20 m^2 g^{-1}) and its larger density than carbon. Usually loadings below 2 μg_{Pt} cm^{-2} are used for identical-location TEM[1,39−41] in order to avoid sample agglomeration on the grid, but this could not be achieved for the Pt/SiC sample. Moreover, platinum completely covers the surface of the SiC support, which makes the use of identical-location TEM difficult. Thus, postmortem TEM has been chosen instead of identical-location TEM to investigate the degradation mechanism.

Postmortem particle histograms along with the TEM micrographs are presented in Figure 5. At first sight, no striking difference can be observed between the TEM images at BOT (Figure 2) and EOT (Figure 5B,D). There is no morphological transformation of the support, which is commonly found in carbon-based materials.[7,32] The platinum

DOI: 10.1021/am508982d
ACS Appl. Mater. Interfaces 2015, 7, 6153−6161

particles appear to be in contact with each other, forming a network similar to that of the TEM micrographs at BOT. Moreover, the platinum particles have not significantly increased in size.

Nonetheless, the platinum particle size histograms show a slight increase in the particle size from 5.8 ± 1.9 to 7 ± 2.2 and 7 ± 3.1 nm for the samples treated with FCCJ protocols I and II, respectively. Likewise, the size distribution increased from 3 to 8.5 to 4−10 nm after aging. The increase in both the particle size and size distribution indicates that the platinum particles are growing in size. In the initial TEM micrographs, 34% of the particles are larger than the average particle size (i.e., 6 nm). However, approximately 85% of the particles are larger than 6 nm after application of the FCCJ protocol I and 75% after application of the FCCJ protocol II. Thus, even though a similar particle average is obtained irrespective of the aging treatment, it seems that an accelerated particle growth occurs during the FCCJ protocol I. The reader should bear in mind that only 9000 cycles were performed using the FCCJ protocol I, whereas the sample was subjected to 30000 cycles of the FCCJ protocol II. It is expected that, if 9000 cycles of FCCJ I resulted in platinum degradation similar to that with 30000 cycles of the FCCJ protocol II, increasing the number of cycles to 30000 cycles of the FCCJ protocol I would lead to a significant difference in the degradation behavior between the two protocols. However, for practical reasons of the required measuring time, this was not feasible. Last but not least, it should be noticed that, throughout the TEM investigations, no platinum particles were observed in the proximity of the support, indicating that there is a reduced corrosion of the platinum−support interface, if any at all.

The surface composition after aging was examined by XPS. Gold is present in the wide XPS survey at EOT (Figure S3 in the SI) in spite of the fact that gold was not observed in the XPS survey before aging. This may be explained by possible gold dissolution and redeposition during the aging treatment, which is in line with previous reports.[42] The platinum elemental composition is 7 and 6% after application of FCCJ protocols I and II, respectively (Table 2). Compared to the XPS before aging, a decrease of approximately 3 and 4% is observed for the sample treated with FCCJ protocols I and II, respectively. Surprisingly, the silicon amount decreases from 33% to 20% and 19% for the samples treated with FCCJ protocols I and II, respectively. It seems that some of the silicon might be leached out of SiC, taking into account that the carbon concentration increases from 29% to 35%, irrespective of the aging treatment (C 1s, Table 2). In addition it is seen that the oxygen content increased from 28% to 38 and 40%, respectively. This was expected because of the harsh oxidizing treatment during aging. The surface composition (as obtained from the XPS survey) shows a large difference between the pristine and aged samples. Nonetheless, the difference is too small between the samples treated with FCCJ protocols I and II to evaluate any surface structure differences. Therefore, high-resolution XPS is imperative for assessing the eventual differences in the surface chemistry.

Table 2. Surface Composition (%) As Determined from the Wide XPS Survey

	C 1s	O 1s	Si 2p	Pt 4f
Pt/SiC-FCCJ I	35	38	20	7
Pt/SiC-FCCJ II	35	40	19	6

According to the high-resolution XPS of C 1s (Figure 6A,B), the concentration of C−Si decreases significantly, while the surface concentration of C−C and OCG increases (Table 3). This can be explained by functionalization with aging or silicon leaching out of the SiC structure. At first sight, functionalization with aging seems a more viable explanation than silicon leaching because of the increase in OCG. According to O 1s, the concentration of O−C exhibits a small decrease, irrespective of the aging treatment. A small decrease in the SiC surface concentration is observed that leads to a small increase in the SiO_2 surface concentration (Si 2p; Table 3). The increase in the C 1s OCG surface concentration is the only argument that points toward the introduction of functional groups, while C 1s SiC and C−C, O 1s, and Si 2p indicate that silicon leaches out. This is in line with previous studies concerned with the SiC corrosion behavior in acidic and alkaline solutions[43] in the absence of platinum. However, functionalization should not be excluded completely, as indicated by the presence of the COOH peak in C 1s (Figure 6A,B), which is completely absent in the pristine sample (Figure 3B). The XPS findings suggest that part of Si−C on the surface leaches out, concomitant with the introduction of functional groups.

The concentration of metallic platinum shows a significant decrease irrespective of the aging protocol. Surprisingly, a larger increase in oxidized platinum is observed for the Pt/SiC-FCCJ protocol I than for the Pt/SiC-FCCJ protocol II. This can be qualitatively assessed from Figure 6C,D, in which the tail toward larger binding energies is more pronounced for the Pt/SiC-FCCJ protocol I (Figure 6C) than for the Pt/SiC-FCCJ protocol II (Figure 6D). It is expected that after application of the Pt/SiC-FCCJ protocol II a larger concentration of oxidized platinum is present because of the presence of a passivating platinum oxide at potentials larger than 1.15 V_{RHE}.[29,32] The upper potential limit in the FCCJ protocol I is 1 V_{RHE}, which is rather close to the place-exchange potential of oxygen and platinum atoms.[44] It is expected that at this potential the oxide is formed only on the top platinum atoms, with a 0.5 ML of oxygen being chemisorbed.[44] Moving toward more positive potentials (i.e., 1.5 V_{RHE}), the place exchange is complete and a Pt−O surface lattice is formed consisting of more than the top ML of platinum atoms. Therefore, after cycling, there are more "new" platinum atoms in FCCJ II than in FCCJ I, which is why there is less Pt^0 in the latter (Table3).

4. CONCLUSIONS

The electrochemical stability of platinized SiC at simulated fuel cell conditions was investigated. Postmortem TEM and XPS were performed to observe the surface chemistry and morphology of the samples after aging.

Postmortem TEM showed that the platinum particle size slightly increases upon application of a degradation protocol. Even though the platinum average size is similar for the samples treated with FCCJ protocols I and II, it seems that, after application of the FCCJ protocol I, a larger number of particles are larger than the initial average size. No direct evidence of support corrosion was observed.

XPS revealed that the surface concentration of metallic platinum decreases with a significant increase of oxidized platinum. Moreover, SiC undergoes mild oxidation during electrochemical stability testing. Reduction in the Si−C

DOI: 10.1021/am508982d
ACS Appl. Mater. Interfaces 2015, 7, 6153−6161

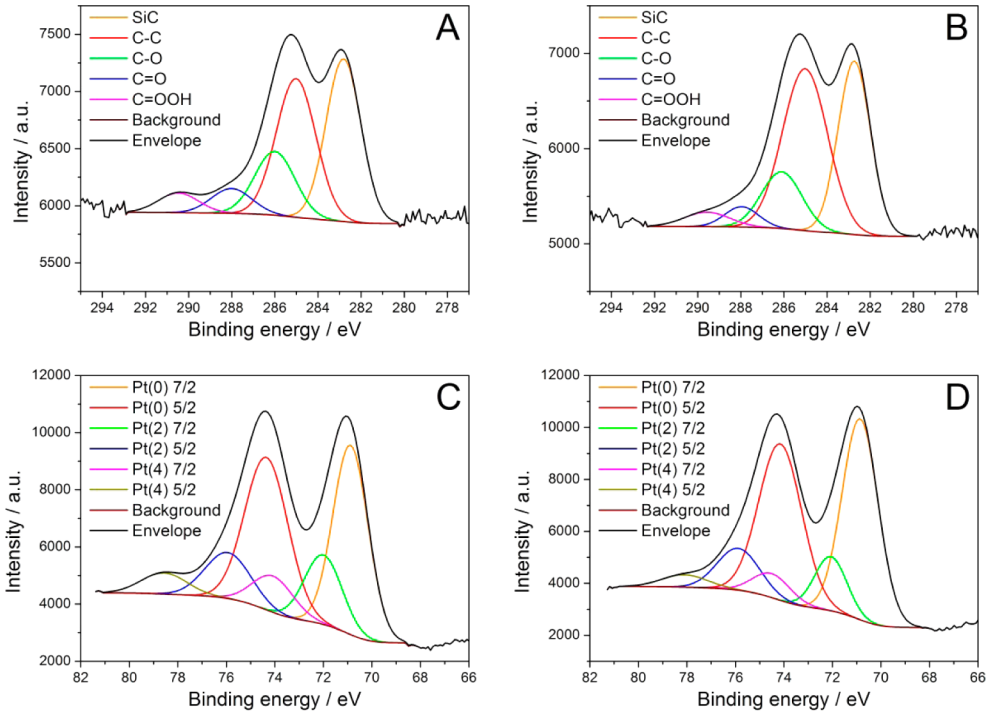

Figure 6. Pt/SiC high-resolution XPS after 9000 cycles of FCCJ I (A and C) and 30000 cycles of FCCJ II (B and D) for C 1s (A and B) and Pt 4f (C and D). FCCJ I: square-wave potential with 3 s step^{-1} (6 s cycle^{-1}) at 0.6 and 1 V_{RHE} in argon-saturated 0.1 M $HClO_4$. FCCJ II: triangular-wave potential between 1 and 1.5 V_{RHE} at 0.5 V s^{-1} in argon-saturated saturated 0.1 M $HClO_4$.

Table 3. Surface Composition (%) As Determined from the High-Resolution Spectra of C 1s, O 1s, Si 2p, and Pt 4f

	C 1s			O 1s		Si 2p		Pt 4f	
	SiC	C−C	OCG	PtO_2	OCG	SiC	SiO_2	Pt^0	Pt−O
Pt/SiC-FCCJ I	37	35	28	19	81	62	38	65	35
Pt/SiC-FCCJ II	34	44	22	16	84	64	36	74	26

bonding in both C 1s and Si 2p spectra is an indication that silicon might leach out or that an extended functionalization occurs with potential cycling.

In summary, Pt/SiC exhibits an improved stability when subjected to a support-oriented aging test, while in simulated load cycle conditions, it behaves similarly to Pt/C. It is still unclear if the silicon is leaching out of the SiC surface or if the decrease in the surface silicon is an indirect consequence of functionalization with aging. Further studies on the electrochemical dissolution of SiC might shed some light on this issue.

■ ASSOCIATED CONTENT

Supporting Information

Particle size histogram of Pt/SiC, SEM images of Pt/SiC, and XPS results at EOT. This material is available free of charge via the Internet at http://pubs.acs.org.

■ AUTHOR INFORMATION

Corresponding Author

*E-mail: rdhiman@sdu.dk. Tel: +45-65503603. Fax: +45-66158760.

Present Address

[§]School of Chemistry, University of Dublin Trinity College, College Green, Dublin 2, Ireland.

Notes

The authors declare no competing financial interest.

■ ACKNOWLEDGMENTS

The authors are thankful to Dr. Per Morgen and Danny Kyrping for advice and technical support. This work has been supported by the Danish projects PEM Durability and Lifetime Part III (Energinet.dk Project 2013-1-12064) and 4M Centre (The Danish Council for Strategic Research Project 12-132710).

■ REFERENCES

(1) Meier, J. C.; Galeano, C.; Katsounaros, I.; Topalov, A. A.; Kostka, A.; Schuth, F.; Mayrhofer, K. J. J. Degradation Mechanisms of Pt/C Fuel Cell Catalysts under Simulated Start−Stop Conditions. *ACS Catal.* **2012**, *2*, 832−843.

(2) Oh, H. S.; Kim, H. Efficient Synthesis of Pt Nanoparticles Supported on Hydrophobic Graphitized Carbon Nanofibers for Electrocatalysts Using Noncovalent Functionalization. *Adv. Funct. Mater.* **2011**, *21*, 3954−3960.

(3) Sebastián, D.; Ruíz, A. G.; Suelves, I.; Moliner, R.; Lázaro, M. J.; Baglio, V.; Stassi, A.; Aricò, A. S. Enhanced Oxygen Reduction Activity and Durability of Pt Catalysts Supported on Carbon Nanofibers. *Appl. Catal., B* **2012**, *115−116*, 269−275.

(4) He, D.; Jiang, Y.; Lv, H.; Pan, M.; Mu, S. Nitrogen-Doped Reduced Graphene Oxide Supports for Noble Metal Catalysts with Greatly Enhanced Activity and Stability. *Appl. Catal., B* **2013**, *132−133*, 379−388.

(5) He, D.; Cheng, K.; Peng, T.; Pan, M.; Mu, S. Graphene/carbon Nanospheres Sandwich Supported PEM Fuel Cell Metal Nanocatalysts with Remarkably High Activity and Stability. *J. Mater. Chem. A* **2013**, *1*, 2126.

(6) Stamatin, S. N.; Borghei, M.; Andersen, S. M.; Veltze, S.; Ruiz, V.; Kauppinen, E.; Skou, E. M. Influence of Different Carbon Nanostructures on the Electrocatalytic Activity and Stability of Pt

DOI: 10.1021/am508982d
ACS Appl. Mater. Interfaces 2015, 7, 6153−6161

Supported Electrocatalysts. *Int. J. Hydrogen Energy* **2014**, *39*, 8215−8224.
(7) Stamatin, S. N.; Borghei, M.; Dhiman, R.; Andersen, S. M.; Ruiz, V.; Kauppinen, E.; Skou, E. M. Activity and Stability Studies of Platinized Multi-Walled Carbon Nanotubes as Fuel Cell Electrocatalysts. *Appl. Catal., B* **2015**, *162*, 289−299.
(8) Wang, Y.; Song, S.; Maragou, V.; Shen, P. K.; Tsiakaras, P. High Surface Area Tungsten Carbide Microspheres as Effective Pt Catalyst Support for Oxygen Reduction Reaction. *Appl. Catal., B* **2009**, *89*, 223−228.
(9) Liu, Y.; Kelly, T. G.; Chen, J. G.; Mustain, W. E. Metal Carbides as Alternative Electrocatalyst Supports. *ACS Catal.* **2013**, *3*, 1184−1194.
(10) Stamatin, S. N.; Skou, E. M. Pt/NbC−N Electrocatalyst for Use in Proton Exchange Membrane Fuel Cells. *ECS Trans.* **2013**, *58*, 1267−1276.
(11) Zhang, L.; Wang, L.; Holt, C. M. B.; Zahiri, B.; Li, Z.; Malek, K.; Navessin, T.; Eikerling, H.; Mitlin, D. Highly Corrosion Resistant Platinum−Niobium Oxide−Carbon Nanotube Electrodes for the Oxygen Reduction in PEM Fuel Cells. *Environ. Sci. Technol.* **2012**, *5*, 6156−6172.
(12) Zhang, N.; Zhang, S.; Du, C.; Wang, Z.; Shao, Y.; Kong, F.; Lin, Y.; Yin, G. Pt/Tin Oxide/Carbon Nanocomposites as Promising Oxygen Reduction Electrocatalyst with Improved Stability and Activity. *Electrochim. Acta* **2014**, *117*, 413−419.
(13) Xu, J.; Aili, D.; Li, Q.; Pan, C.; Christensen, E.; Jensen, J. O.; Zhang, W.; Liu, G.; Wang, X.; Bjerrum, N. J. Antimony Doped Tin Oxide Modified Carbon Nanotubes as Catalyst Supports for Methanol Oxidation and Oxygen Reduction Reactions. *J. Mater. Chem. A* **2013**, *1*, 9737.
(14) Yang, M.; Van Wassen, A. R.; Guarecuco, R.; Abruña, H. D.; DiSalvo, F. J. Nano-Structured Ternary Niobium Titanium Nitrides as Durable Non-Carbon Supports for Oxygen Reduction Reaction. *Chem. Commun.* **2013**, *49*, 10853−10855.
(15) Jing, S.; Luo, L.; Yin, S.; Huang, F.; Jia, Y.; Wei, Y.; Sun, Z.; Zhao, Y. Tungsten Nitride Decorated Carbon Nanotubes Hybrid as Efficient Catalyst Supports for Oxygen Reduction Reaction. *Appl. Catal., B* **2014**, *147*, 897−903.
(16) Honji, A.; Marl, T.; Hishinuma, Y.; Kurita, K. Platinum Supported on Silicon Carbide as Fuel Cell Electrocatalyst. *J. Electrochem. Soc.* **1988**, *135*, 917−918.
(17) Venkateswara, C.; Singh, S. K.; Viswanathan, B. Electrochemical Performance of Nano-SiC Prepared in Thermal Plasma. *Indian J. Chem.* **2008**, *47*, 1619−1625.
(18) Lv, H.; Mu, S.; Cheng, N.; Pan, M. Nano-Silicon Carbide Supported Catalysts for PEM Fuel Cells with High Electrochemical Stability and Improved Performance by Addition of Carbon. *Appl. Catal., B* **2010**, *100*, 190−196.
(19) Zang, J.; Dong, L.; Jia, Y.; Pan, H.; Gao, Z.; Wang, Y. Core−Shell Structured SiC@C Supported Platinum Electrocatalysts for Direct Methanol Fuel Cells. *Appl. Catal., B* **2014**, *144*, 166−173.
(20) Dong, L.; Zang, J.; Su, J.; Jia, Y.; Wang, Y.; Lu, J.; Xu, X. Oxidized Carbon/Nano-SiC Supported Platinum Nanoparticles as Highly Stable Electrocatalyst for Oxygen Reduction Reaction. *Int. J. Hydrogen Energy* **2014**, *39*, 16310−16317.
(21) Pourbaix, M. *Atlas of Electrochemical Equilibria in Aqueous Solutions*, 2nd ed.; Association of Corrosion Engineers: Houston, TX, 1974.
(22) Zhang, Y.; Zang, J.; Dong, L.; Cheng, X.; Zhao, Y.; Wang, Y. A Ti-Coated Nano-SiC Supported Platinum Electrocatalyst for Improved Activity and Durability in Direct Methanol Fuel Cells. *J. Mater. Chem. A* **2014**, *2*, 10146.
(23) Liu, Y.; Mustain, W. E. Structural and Electrochemical Studies of Pt Clusters Supported on High-Surface-Area Tungsten Carbide for Oxygen Reduction. *ACS Catal.* **2011**, *1*, 212−220.
(24) Dhiman, R.; Johnson, E.; Skou, E. M.; Morgen, P.; Andersen, S. M. SiC Nanocrystals as Pt Catalyst Supports for Fuel Cell Applications. *J. Mater. Chem. A* **2013**, *1*, 6030.
(25) Dhiman, R.; Stamatin, S. N.; Andersen, S. M.; Morgen, P.; Skou, E. M. Oxygen Reduction and Methanol Oxidation Behaviour of SiC Based Pt Nanocatalysts for Proton Exchange Membrane Fuel Cells. *J. Mater. Chem. A* **2013**, *1*, 15509.
(26) Dhiman, R.; Petrunin, V.; Rana, K.; Morgen, P. Conversion of Wooden Structures into Porous SiC with Shape Memory Synthesis. *Ceram. Int.* **2011**, *37*, 3281−3289.
(27) Teranishi, T.; Hosoe, M.; Tanaka, T.; Miyake, M. Size Control of Monodispersed Pt Nanoparticles and Their 2D Organization by Electrophoretic Deposition. *J. Phys. Chem. B* **1999**, *103*, 3818−3827.
(28) Mayrhofer, K. J. J.; Ashton, S. J.; Kreuzer, J.; Arenz, M. An Electrochemical Cell Configuration Incorporating an Ion Conducting Membrane Separator between Reference and Working Electrode. *Int. J. Electrochem. Sci.* **2009**, *4*, 1−8.
(29) Ohma, A.; Shinohara, K.; Iiyama, A.; Yoshida, T.; Daimaru, A. Membrane and Catalyst Performance Targets for Automotive Fuel Cells by FCCJ Membrane, Catalyst, MEA WG. *ECS Trans.* **2011**, *41*, 775−784.
(30) Mayrhofer, K. J. J.; Strmcnik, D.; Blizanac, B. B.; Stamenkovic, V.; Arenz, M.; Markovic, N. M. Measurement of Oxygen Reduction Activities via the Rotating Disc Electrode Method: From Pt Model Surfaces to Carbon-Supported High Surface Area Catalysts. *Electrochim. Acta* **2008**, *53*, 3181−3188.
(31) Prado-Burguete, C.; Linares-Solano, A.; Rodriguez-Reinoso, F.; Salinas-Martinez de Leca, C. The Effect of Oxygen Surface Groups of the Support Dispersion in Pt/Carbon Catalysts on Platinum. *J. Catal.* **1989**, *115*, 98−106.
(32) Zana, A.; Speder, J.; Roefzaad, M.; Altmann, L.; Baumer, M.; Arenz, M. Probing Degradation by IL-TEM: The Influence of Stress Test Conditions on the Degradation Mechanism. *J. Electrochem. Soc.* **2013**, *160*, F608−F615.
(33) Speder, J.; Zana, A.; Spanos, I.; Kirkensgaard, J. J. K.; Mortensen, K.; Arenz, M. On the Influence of the Pt to Carbon Ratio on the Degradation of High Surface Area Carbon Supported PEM Fuel Cell Electrocatalysts. *Electrochem. Commun.* **2013**, *34*, 153−156.
(34) Zana, A.; Rüdiger, C.; Kunze-Liebhäuser, J.; Granozzi, G.; Reeler, N. E. A.; Vosch, T.; Kirkensgaard, J. J. K.; Arenz, M. Core−Shell TiO_2@C: Towards Alternative Supports as Replacement for High Surface Area Carbon for PEMFC Catalysts. *Electrochim. Acta* **2014**, *139*, 21−28.
(35) Park, Y.-C.; Kakinuma, K.; Uchida, M.; Tryk, D. A.; Kamino, T.; Uchida, H.; Watanabe, M. Investigation of the Corrosion of Carbon Supports in Polymer Electrolyte Fuel Cells Using Simulated Start-Up/shutdown Cycling. *Electrochim. Acta* **2013**, *91*, 195−207.
(36) Zana, A.; Speder, J.; Reeler, N. E. a; Vosch, T.; Arenz, M. Investigating the Corrosion of High Surface Area Carbons during Start/stop Fuel Cell Conditions: A Raman Study. *Electrochim. Acta* **2013**, *114*, 455−461.
(37) Shao-Horn, Y.; Sheng, W. C.; Chen, S.; Ferreira, P. J.; Holby, E. F.; Morgan, D. Instability of Supported Platinum Nanoparticles in Low-Temperature Fuel Cells. *Top. Catal.* **2007**, *46*, 285−305.
(38) Speder, J.; Zana, A.; Spanos, I.; Kirkensgaard, J. J. K.; Mortensen, K.; Hanzlik, M.; Arenz, M. Comparative Degradation Study of Carbon Supported Proton Exchange Membrane Fuel Cell Electrocatalysts—The Influence of the Platinum to Carbon Ratio on the Degradation Rate. *J. Power Sources* **2014**, *261*, 14−22.
(39) Schlögl, K.; Mayrhofer, K. J. J.; Hanzlik, M.; Arenz, M. Identical-Location TEM Investigations of Pt/C Electrocatalyst Degradation at Elevated Temperatures. *J. Electroanal. Chem.* **2011**, *662*, 355−360.
(40) Perez-Alonso, F. J.; Elkjær, C. F.; Shim, S. S.; Abrams, B. L.; Stephens, I. E. L.; Chorkendorff, I. B. Identical Locations Transmission Electron Microscopy Study of Pt/C Electrocatalyst Degradation during Oxygen Reduction Reaction. *J. Power Sources* **2011**, *196*, 6085−6091.
(41) Dubau, L.; Castanheira, L.; Berthomé, G.; Maillard, F. An Identical-Location Transmission Electron Microscopy Study on the Degradation of Pt/C Nanoparticles under Oxidizing, Reducing and Neutral Atmosphere. *Electrochim. Acta* **2013**, *110*, 273−281.

DOI: 10.1021/am508982d
ACS Appl. Mater. Interfaces 2015, 7, 6153−6161

(42) Cherevko, S.; Zeradjanin, A. R.; Topalov, A. A.; Kulyk, N.; Katsounaros, I.; Mayrhofer, K. J. J. Dissolution of Noble Metals during Oxygen Evolution in Acidic Media. *ChemCatChem* **2014**, *6*, 2219−2223.
(43) Andrews, A.; Herrmann, M.; Sephton, M.; Machio, C.; Michaelis, A. Electrochemical Corrosion of Solid and Liquid Phase Sintered Silicon Carbide in Acidic and Alkaline Environments. *J. Eur. Ceram. Soc.* **2007**, *27*, 2127−2135.
(44) Jerkiewicz, G.; Vatankhah, G.; Lessard, J.; Soriaga, M. P.; Park, Y.-S. Surface-Oxide Growth at Platinum Electrodes in Aqueous H_2SO_4: Reexamination of Its Mechansim through Combined Cyclic-Voltammetry, Electrochemical Quarts-Crystal Nanobalance, and Auger Electron Spectroscopy Measurements. *Electrochim. Acta* **2004**, *49*, 1451−1459.

DOI: 10.1021/am508982d
ACS Appl. Mater. Interfaces 2015, 7, 6153−6161